Antiferroelectric Multilayers: a Multifunctional Platform for Energy and Information Storage

Hung-Wei Li, Sadegh Kamaei, Cyrille Masserey, Pascal Morel, Niccolò Martinolli, Tom Schlatter, Océane Mauroux, Igor Stolichnov, and Adrian M. Ionescu.
EPFL, Nanoelectronic Devices Laboratory (NanoLab), 1015, Lausanne, Switzerland

***Abstract*— This work demonstrates the integration of energy storage and multi-bit memory functionalities in a single platform device using multilayer dielectric (DE) with ferroelectric (FE) or antiferroelectric (AFE) materials. Employing a hafnium-based oxide, we achieve an energy storage density of approximately 50 J/cm^3 and advanced multi-bit storage capabilities. We investigate the effects of adjusting silicon doping concentration in multilayer Si:HfO_2 during the atomic layer deposition (ALD) process to form and compare both FE and AFE layers. Inserting an Al_2O_3 dielectric (DE) layer between the FE or AFE layers, we create a built-in electric field, enhancing both energy storage efficiency and multi-bit memory storage beyond the current state of the art. Our innovative approach harnesses the intrinsic properties of these materials to boost energy efficiency and data storage capacity, significantly improving device functionality and advancing electronic component design. Our results reveal that strategically layering DE with AFE materials enhances energy and multi-bit storage, opening new avenues for future multifunctional electronic applications.**

I. Introduction

Hafnium oxide-based ferroelectric (FE) and antiferroelectric (AFE) thin films are emerging as key materials in the evolution of advanced memory and energy storage technologies. Integrating these materials into commercially viable devices demands not only comprehensive material characterization but also innovative engineering to enhance both endurance and performance. This study introduces a groundbreaking device that seamlessly integrates high-density energy storage with robust multi-bit memory functionality within a techmological framework. Utilizing multilayer configurations of dielectric (DE), FE, and AFE materials, we have achieved an unprecedented energy density of approximately 50 J/cm^3, coupled with enhanced multi-bit storage capabilities. This advancement is made possible through meticulous control of silicon doping in Si:HfO_2 during atomic layer deposition (ALD), allowing for the precise formation of distinct FE and AFE phases. A key innovation in our device is the incorporation of an Al_2O_3 dielectric layer between the FE and AFE layers, which generates a built-in electric field. This field significantly boosts energy storage efficiency while simultaneously stabilizing data retention in multi-bit memory configurations (Fig. 1). As the demand for ultracompact electronic devices increases, particularly in wearable and implantable technologies, our research addresses the *multi-functional need for devices that not only store energy efficiently but also retain data reliably*. The miniaturized energy autonomous systems enabled by this technology will integrate energy harvesting and storage with memory, offering a comprehensive solution for long-term, reliable device operation. Our findings not only demonstrate substantial improvements in energy and memory performance but also pave the way for the development of next-generation electronic components.

II. Device Fabrication Process

A. Tailoring silicon doped hafnium oxide properties

In the ALD process for Si:HfO_2 thin films, adjusting the SiO_2 and HfO_2 cycle ratios (Fig. 2a) yields either ferroelectric (FE) or antiferroelectric (AFE) behavior [1]. The metal-ferroelectric-metal (MFM) capacitor exhibits ferroelectric (Fig. 2(b)) or antiferroelectric (Fig. 2(c)) behavior depending on the SiO_2 doping concentration.

B. FeCap fabrication

The fabrication process for the multilayer capacitors illustrated in Fig. 3(a). We begin by preparing a silicon substrate with a 200-nm thermally grown SiO_2 layer on both sides. After the standard cleaning process, the bottom electrodes composed of titanium (Ti) and platinum (Pt) were deposited by sputtering. Without breaking the vacuum, we sputter a titanium nitride (TiN) layer. The multi-layer structure is then created through ALD. Table 1 provides details on the various sample configurations. For consistency in comparison, we maintained the overall thickness of FE/AFE layers at 40 nm across all samples. After the multi-layer structure is complete, we deposit a second TiN and the entire stack then undergoes a rapid thermal annealing (RTA) in a nitrogen atmosphere. This step is crucial in achieving the desired orthorhombic crystalline phase, which is essential for tuning the FE or AFE properties of our device. The final stage of fabrication involves defining individual capacitors, by sputtering Ti and Pt layers, followed by a ion beam etching (IBE) process. This results in capacitors with a well-defined area of in the range of 100 μm^2 for characterization and performance evaluation.

III. Results and Discussion

A. Multi-layer Capacitor Characterization

Fig 5 illustrates the experimental hysteresis curves of dielectric and ferroelectric behaviors in fabricated multilayer

capacitors, highlighting the influence of interfacial engineering and material composition on electrical properties. Fig. 5(a) and (b) show the polarization-electric field (P-E) curves for DE1FE10×4 and DE1AFE10×4, respectively. The P-E curve for DE1FE10×4 displays characteristic ferroelectric behavior with suppressed remanent polarization (P_r), attributed to the dielectric layer's effect on ferroelectric switching. While the MFM capacitor exhibits a $2P_r$ of 40 μC/cm^2, DE1FE10×4 shows a reduced $2P_r$ of 20 μC/cm^2. The P-E curve of DE1AFE10×4 demonstrates antiferroelectric characteristics and the versatility of layering strategies in tailoring material properties. The observed crossover of capacitance-voltage (C-V) branches (Figs 5(c) and (d)) at a non-zero electric field indicates the presence of a built-in electric field, likely resulting from asymmetric charge distributions or interfacial dipole moments within the multilayer structure. Fig. 6(a) and (b), representing DE1FE5×8 and DE1AFE5×8 respectively, demonstrate how a thicker dielectric layer alters the P-E response. This is evident from the linear capacitor behavior observed at lower electric fields, which also contributes to an increase in the electric breakdown voltage at high electric fields.

B. Energy storage enhancement with multilayered AFE/FE

Fig. 7(b) and (c) compares energy storage capabilities of ferroelectric (FE) and antiferroelectric (AFE) multilayers. Our work demonstrated that AFE materials exhibit superior performance due to their unique phase transition properties. Energy storage is calculated from the area under the P-E curve, revealing total stored energy and hysteresis losses (Fig 7(a)). This method highlights fundamental differences in dipole behavior between FE and AFE materials under electric fields. FE multilayers like DE10FE12×2 achieve energy densities up to 30 – 40 J/cm^3 but are limited by breakdown electric field. In contrast, AFE multilayers, particularly DE1AFE10×4, exceed 60 J/cm^3 with efficiencies up to 80% at 3 MV/cm. This performance stems from AFE materials' ability to *switch between non-polar and polar states*, allowing for controlled energy discharge. To further increase the breakdown voltage, we compared more stacks of the multilayer. However, while increasing the number of layers achieves a higher breakdown voltage, it also results in lower energy density. Both phenomena can be observed in FE and AFE devices, which is due to the more pronounced DE contribution suppressing the dipole from FE and AFE layers. Unlike the rapid discharge in ferroelectrics, AFE materials demonstrate *controlled energy release*. This driven by reversible phase transitions, enhancing energy storage capacity and efficiency, and making AFE multilayers suitable for applications requiring efficient, high-density energy storage. Charge-discharge characteristics of FE and AFE multilayer capacitors, providing insights into their practical performance. The setup uses a DC power supply and controlled discharge through a resistor to simulate real-world conditions (Fig. 8(a)). The voltage-time curves in Fig. 8(b) and 8(c) compare different multilayer configurations during charge-discharge cycles, using a 2.2 nF capacitor as a reference which is close to the maximum capacitance (Fig.5 (d)) we can obtain from AFE device. FE structures display rapid voltage decay, typical of quick energy release due to polarization switching, with DE1FE10×4 showing a slightly slower but still significant drop from 15V to near 0V within about 100 μs. In contrast, AFE structures exhibit more controlled voltage decay, with DE1AFE10×4 maintaining higher voltage for longer. This confirms the superior performance of AFE materials in controlled energy release, making them ideal for applications requiring energy efficiency and longevity. Fig. 9 demonstrates the long-term stability of AFE materials under extensive field cycling, crucial for durable energy storage applications.

C. Multibit memory storage enabled by multilayered AFE/FE

FORC measurements (Fig. 9(a-f)) offer insights into the switching behavior of these materials. By inserting the DE layer, the current peaks can be finely tuned due to the built-in electric field (Fig. 9(b)). The DE1FE10×4 structure shows typical ferroelectric hysteresis with distinct current peaks at coercive fields. The presence of the DE layer subtly shifts these coercive fields closer to ±2 MV/cm. Integrating DE layers making DE1FE10×4 suitable for memory and energy storage technologies with fast response times and improved endurance. For DE1AFE10×4 (Fig. 9(e)), the FORC diagram reveals a shift in current peaks towards the same field polarity, a phenomenon not observed without the DE layer. This shift, caused by the DE layer's influence on the internal electric field, indicates multibit nonvolatile properties. By stabilizing specific states, this shift ensures reliable quaternary multibit memory operations. The read-out transient current data further supports these findings (Fig. 11). A ±12V pulse switches one peak, while a ±20V pulse switches both, with the current in the mA range. This demonstrates precise control, enabling accurate multibit memory storage and retrieval. The C-V characteristics of AFE materials (Fig. 12) display a double-peak butterfly shape with significant frequency dispersion, indicating rapid switching speeds in DE+AFE structures.

IV. Conclusion

This study comprehensively analyzes for the first time the energy storage capabilities, switching behavior, and memory performance of ferroelectric (FE) and antiferroelectric (AFE) multilayer capacitors. Through detailed charge-discharge measurements, C-V characteristics, and FORC analysis, it is demonstrated that *AFE multilayers exhibit superior energy storage capacity, controlled energy release, and enhanced nonvolatile properties compared to FE structures*. These advantages position AFE materials as a promising platform candidate for next-generation advanced electronic devices with multifunctional energy storage and memory capability.

References

[1] T. Boscke, et al, *Applied Physics Letters*, vol. 99, 2011. [2] F. Ali, et al, . *J Appl Phys* , vol. 122, 2017. [3] J. P. B. Silva, et al, *J Mater Chem A*, vol. 8, 2020. [4] Cheema, S. S., et al, *Nature*, 2024.

Multilayer Structure Fabrication Process

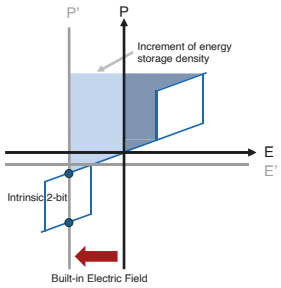

Fig 1. Schematic illustration of the qualitative P-E loop for the multilayer metal-insulator-ferro-electric-metal (MIFM) capacitor structure. The integration of a dielectric (DE) layer with antiferroelectric (AFE) or ferroelectric (FE) materials introduces a built-in electric field. This field significantly enhances the energy storage density and enables multi-bit memory functionality within the same MIFM capacitor structure, optimizing both memory capacity

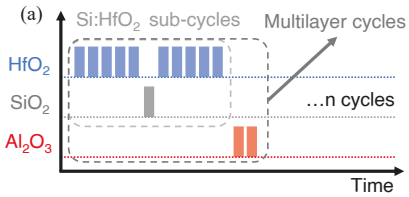

Fig 2. (a) ALD process schematic for Si:HfO_2 thin films. Si:HfO_2 sub-cycle ratio adjustments yield FE or AFE behavior.

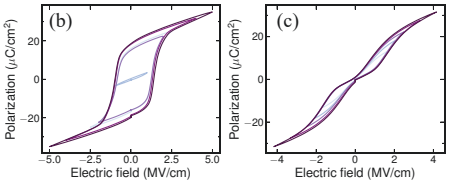

P-E hysteresis loops of MFM capacitors: (b) 3.12% Si concentration (ferroelectric), (c) 5% Si concentration (antiferroelectric).

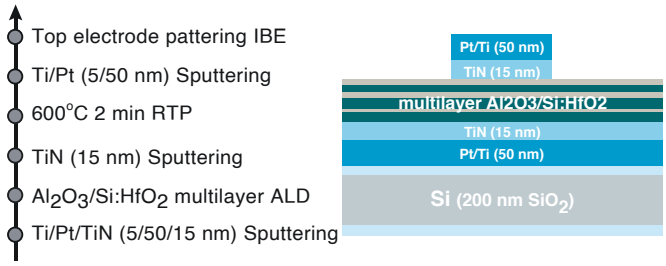

Fig 3. Key fabrication steps for the multilayer capacitor structure. The ALD multilayer cycles are adjusted to achieve different material combinations in the multilayer structure.

Sample ID	T_{AlO} (nm)	T_{SiHfO} (nm)	Layer numbers	Si:HfO_2 properties
DE10FE10x2	10	10	2	Ferroelectric
DE1FE10x4	1	10	4	Ferroelectric
DE1FE8x5	1	8	5	Ferroelectric
DE1FE5x8	1	5	8	Ferroelectric
DE1AFE10x4	1	10	4	Antiferroelectric
DE1AFE8x5	1	8	5	Antiferroelectric
DE1AFE5x8	1	5	8	Antiferroelectric

Fig 4. The tables summarize key samples, providing its thickness of each layer and the ferroelectric/antiferroelectric properties.

Experimental Device Characterisitics

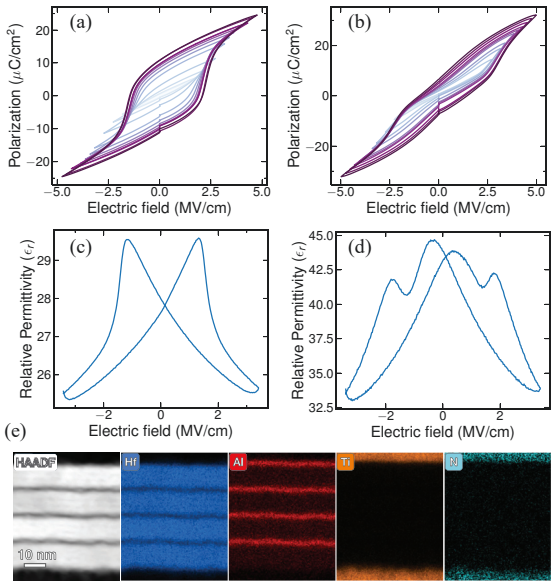

Fig 5. (a) P-E curve of DE1FE10x4 showing typical ferroelectric behavior, with suppressed remanent polarization due to the dielectric layer's contribution. (b) P-V curve of DE1AFE10x4 demonstrating antiferroelectric characteristics. (c) Butterfly-like dielectric response of the FE capacitor after interfacial engineering of interlayers, with a crossover of C-V branches at a non-zero electric field indicating a built-in field. (d) Butterfly-like dielectric response of the AFE capacitor under similar conditions, also showing a crossover due to a built-in field. (e) TEM image and EDS results for the multilayer structure, providing a detailed view of the material composition and interfaces.

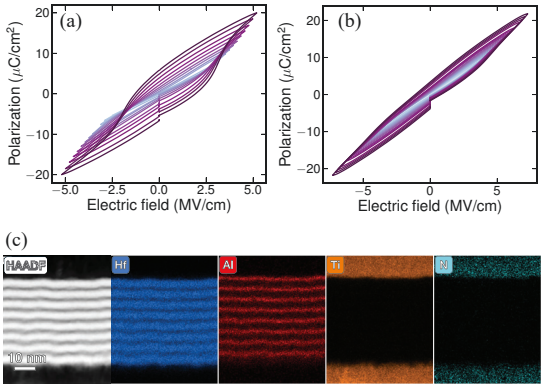

Fig 6. (a) P-E curve of DE1FE5x8, showing ferroelectric properties with a noticeable linear capacitor response at low electric fields due to the increased dielectric layer contribution. (b) P-V curve of DE1AFE5x8, also exhibiting a linear capacitor response at low electric fields, influenced by the dielectric layer. (c) TEM image and EDS results, providing detailed insights into the material structure and composition.

Experimental Device Characterisitics: Energy Storage Density

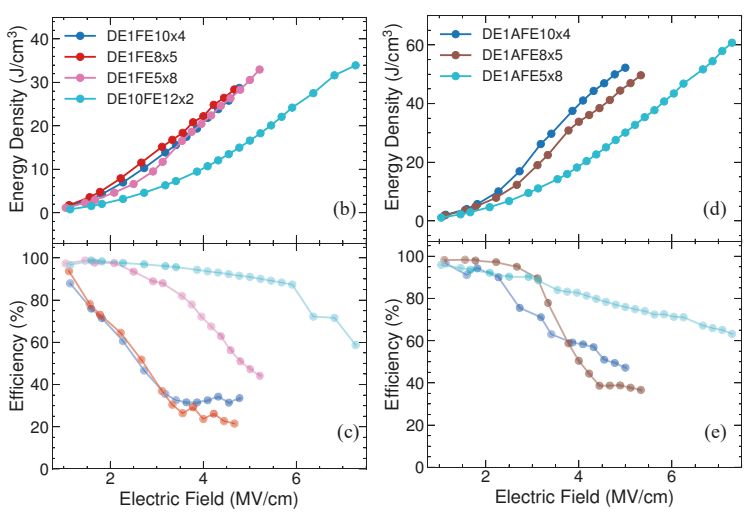

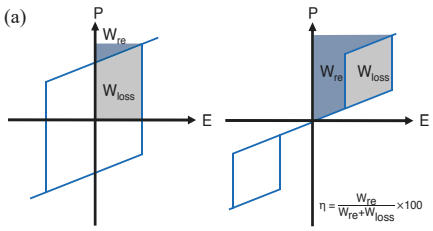

Fig 7. (a) Calculation of energy density and efficiency derived from the P-E loop, involving the integration of the area under the polarization-electric field curve to assess the energy stored and the corresponding efficiency based on energy loss. (b, c) Energy density versus electric field plots for ferroelectric multilayers, showing the material's capacity to store more energy when adjusting the inserting DE layers. (d, e) Similar plots for antiferroelectric multilayers, highlighting the distinct energy storage characteristics compared to their ferroelectric counter-parts, including differences in energy density and efficiency.

Charge - Discharge Measurement

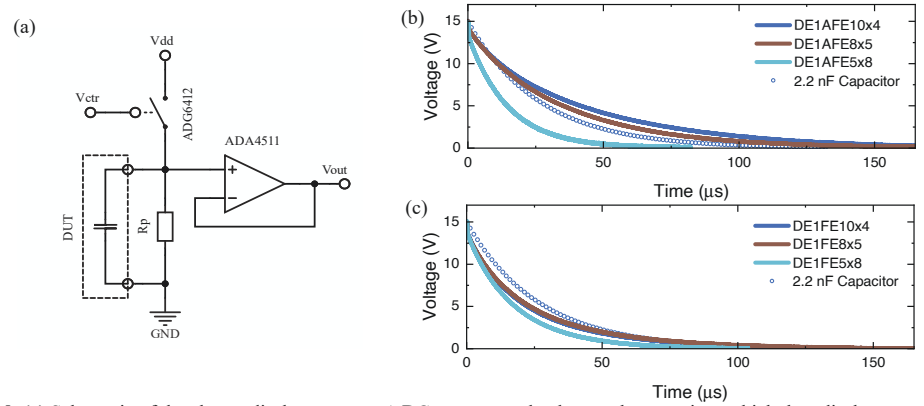

Fig 8. (a) Schematic of the charge-discharge setup: A DC power supply charges the capacitor, which then discharges through a 12 kΩ resistor. The pulse duration (10 µs) is controlled by a switch (ADG6412), and the voltage is monitored using an oscilloscope. A follower (ADA4511) reduces the parastics from the oscilloscope. (b, c) Comparison of discharge curves for ferroelectric and antiferroelectric multilayer structures with those of an ideal 2.2 nF capacitor. These simulated values are used as a reference to assess the performance of the multilayer structures.

Endurance

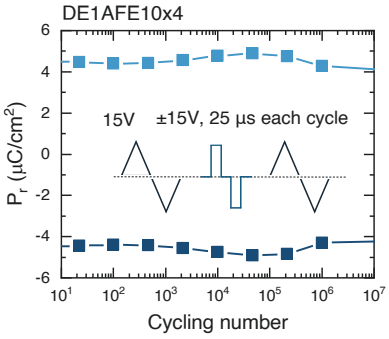

Fig 9. The device demonstrates fatigue-free behavior during field cycling, benefiting from the intrinsic properties of the antiferroelectric (AFE) material.

First-order Reversal Curve (FORC)

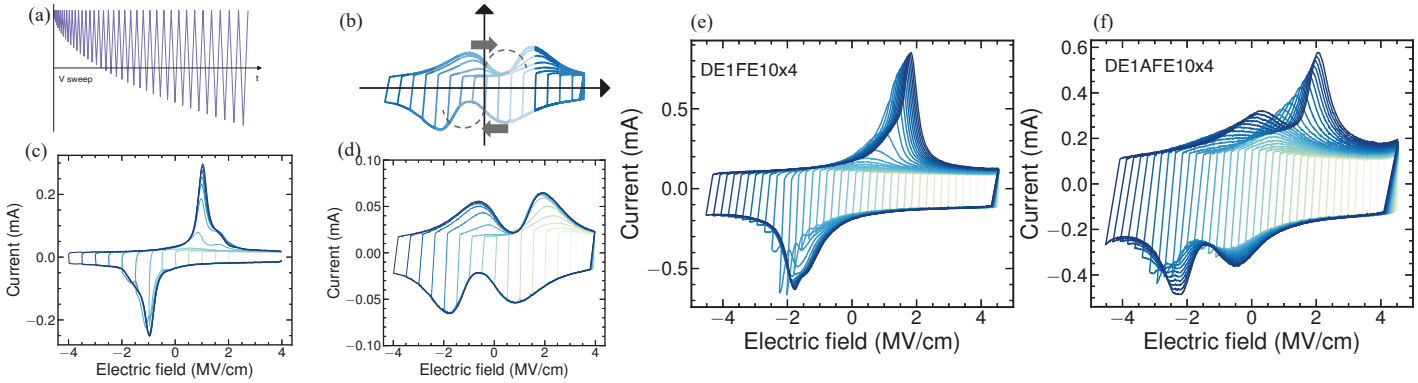

Fig 10 (a) Schematic outlining the First-order Reversal Curve (FORC) measurement approach. The applied field is swept from positive saturation to a reversal point, then back to positive saturation. This process is repeated for multiple reversal points to generate a series of curves that together form a comprehensive map of the material's electric behavior. (b) Schematic of AFE with DE multilayer, the current peaks will shift. FORC result of the MFM capacitors exhibiting (c) FE properties and (d) AFE properties. (e) FORC results showing the effect of the DE layer on the FE multilayer capacitor, illustrating changes in the coercive field and interaction fields due to the DE layer. (f) FORC result of the AFE multilayer capacitor with a DE interlayer, where the addition causes the two peaks at opposite field polarities to shift toward the same polarity, indicating multi-bit nonvolatile properties. This shift suggests a modification in the energy landscape of the AFE material due to the presence of DE layers.

Multi-bit Cell Write and Read

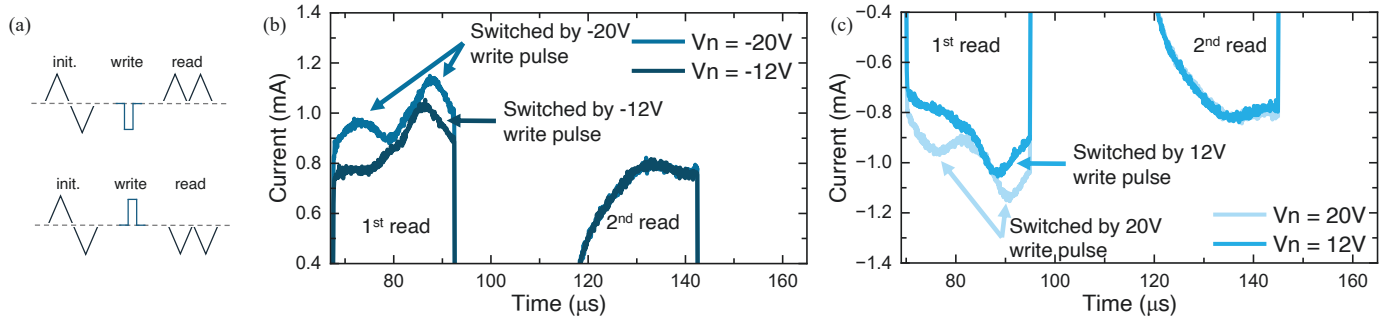

Fig. 11 (a) Schematic of the pulse sequence used to verify the write operation. After the write operation, two pulses (18V) with opposite polarity are applied to read out the switching polarization achieved during the write process. (b, c) Read-out transient current for different write pulse levels. The results show that a ± 12 V pulse can switch only one peak, while a ±20V pulse can switch both peaks, demonstrating the control over the switching behavior with varying pulse levels.

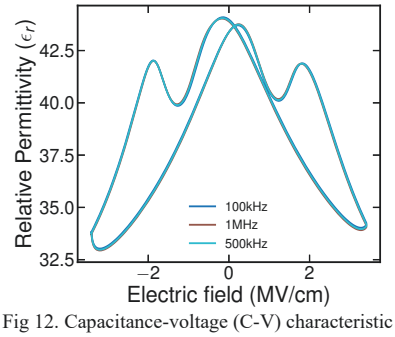

Fig 12. Capacitance-voltage (C-V) characteristic showing a double-peak antiferroelectric (AFE) butterfly shape. The robust frequency dispersion observed indicates a fast switching speed in the multilayer DE AFE structure.

	Material	ESD (J/cm³)	Efficiency	Memory and Energy Storage Integration
F. Ali, et al [2]	Si-HfO_2	61	65%	-
J. P. B. Silva, et al [3]	Al_2O_3: DIL-$Hf_{0.5}Zr_{0.5}O_2$	54	51%	-
Cheema, S. S. et al [4]	HfO_2/ZrO_2	115	90%	-
This work	Al_2O_3/Si:HfO_2	50	80%	Yes

Table 2. Benchmarking of various on-chip CMOS compatible energy storage capacitors.